JSHC
Japan Society of Histochemistry and Cytochemistry
Established 1959

Acta Histochem. Cytochem. 57 (5): 175–188, 2024
doi: 10.1267/ahc.24-00046

Regular Article

Effect of Hepatic Lipid Overload on Accelerated Hepatocyte Proliferation Promoted by HGF Expression via the SphK1/S1PR2 Pathway in MCD-diet Mouse Partial Hepatectomy

Baljinnyam Lkham-Erdene[1,2], Narantsog Choijookhuu[1,3], Toshiki Kubota[1,4], Tomofumi Uto[5], Shuya Mitoma[5], Shinichiro Shirouzu[1,4], Takumi Ishizuka[1], Kengo Kai[1], Kazuhiro Higuchi[1,6], Kham Mo Aung[1], Jargal-Erdene Batmunkh[1], Katsuaki Sato[5] and Yoshitaka Hishikawa[1]

[1]Department of Anatomy, Histochemistry and Cell Biology, Faculty of Medicine, University of Miyazaki, 5200 Kihara, Kiyotake, Miyazaki 889–1692, Japan, [2]Thoracic surgery department, National Cancer Center, Ulaanbaatar, Mongolia, [3]Department of Pathology and Forensic Medicine, School of Biomedicine, Mongolian National University of Medical Sciences, Ulaanbaatar, Mongolia, [4]Department of Oral and Maxillofacial Surgery, Faculty of Medicine, University of Miyazaki, 5200 Kihara, Kiyotake, Miyazaki 889–1692, Japan, [5]Division of Immunology, Department of Infectious diseases, Faculty of Medicine, University of Miyazaki, 5200 Kihara, Kiyotake, Miyazaki 889–1692, Japan and [6]Department of Surgery, Faculty of Medicine, University of Miyazaki, 5200 Kihara, Kiyotake, Miyazaki 889–1692, Japan

Received September 1, 2024; accepted September 17, 2024; published online October 23, 2024

Metabolic dysfunction-associated steatotic liver disease (MASLD) is becoming a major health problem worldwide. Liver regeneration is crucial for restoring liver function, and is regulated by extraordinary complex process, involving numerous factors under both physiologic and pathologic conditions. Sphingosine-1-phosphate (S1P), a bioactive sphingolipid synthesized by sphingosine kinase 1 (SphK1), plays an important role in liver function through S1P receptors (S1PRs)-expressing cells. In this study, we investigated the effect of lipid overload on hepatocyte proliferation in a mouse hepatic steatosis model induced by feeding a methionine- and choline-deficient (MCD) diet. After 50% partial hepatectomy (PHx), liver tissues were sampled at various timepoints and then analyzed by immunohistochemistry, oil Red-O staining, quantitative-polymerase chain reaction (qPCR), and flow cytometry. In mice fed the MCD-diet, significantly exacerbated hepatic steatosis and accelerated liver regeneration were observed. After PHx, hepatocyte proliferation peaked at 48 and 36 hr in the liver of chow- and MCD-diet fed mice, respectively. By contrast, increased expression of S1PR2 was observed in hepatic neutrophils and macrophages of MCD-diet fed mice. Flow cytometry and qPCR experiments demonstrated that levels of HGF and FGF2 released by neutrophils and macrophages were significantly higher in MCD-diet fed mice. In conclusion, hepatic lipid overload recruits Kupffer cells and neutrophils that release HGF and FGF2 via SphK1/S1PR2 activation to accelerate hepatocyte proliferation.

Key words: lipid overload, fatty acid accumulation, liver regeneration, metabolic dysfunction-associated steatotic liver disease, sphingosine-1-phosohate

Correspondence to: Yoshitaka Hishikawa, M.D., Ph.D., Department of Anatomy, Histochemistry and Cell Biology, Faculty of Medicine, University of Miyazaki, 5200 Kihara, Kiyotake, Miyazaki 889–1692, Japan. E-mail: yhishi@med.miyazaki-u.ac.jp

I. Introduction

Metabolic dysfunction-associated steatotic liver disease (MASLD) formerly known as non-alcoholic fatty liver disease is the most common parenchymal liver condition

© 2024 The Japan Society of Histochemistry and Cytochemistry

and becoming a major health problem worldwide. The progression of MASLD to non-alcoholic steatohepatitis is characterized by steatosis with hepatocellular injury and inflammation, and this condition is now known as metabolic dysfunction-associated steatohepatitis (MASH) [9, 38, 39, 48]. Histopathologically, the infiltration of steatosis is classified into three categories: an initial stage characterized by mild steatosis, a moderate stage in which 30–60% of hepatocytes are affected, and severe steatosis (>60% of hepatocytes affected) [49]. Methionine- and choline-deficient (MCD) diet has been widely used to induce hepatic steatosis in experimental animals, which is relevant to mimic the histopathological features of human MASLD.

The liver has a unique ability to regenerate and recover from injury under both physiologic and pathologic conditions. A thorough understanding of the physiologic and pathologic features of liver regeneration in clinical practice is crucial in order to minimize surgical treatment-related complications. Partial hepatectomy (PHx) and liver transplantation are curative treatment options for the hepatocellular carcinoma (HCC) and some severe liver diseases [7, 25, 35, 52]. Transient regeneration-associated steatosis is a significant early physiologic change in liver regenerating after PHx. The accumulated lipid droplets (LD) become energy supply to promote liver regeneration. Moreover, fatty acids serve as lipid resources for the synthesis of daughter cell membranes [8, 14, 32, 37, 41]. PHx-induced liver regeneration is well known complex process consisting of priming, proliferation and termination phases [33, 35, 41]. However, the role of hepatic steatosis is still controversial. In the priming phase, changes in innate immunity and cytokine storm occurs; the recruitment of neutrophils and monocytes peaks within hours in response to tissue damage. The pro-inflammatory role of neutrophils has been extensively studied, and closely related to the development of MASH [3, 53]. On the other hand, neutrophils also play a crucial role in tissue repair and angiogenesis by releasing various growth factors, including hepatocyte growth factor (HGF), fibroblast growth factor-2 (FGF-2), and vascular endothelial growth factor [5]. However, the impact of neutrophils in liver regeneration remains largely unknown.

Sphingolipids are essential lipid components of the cellular membrane and function as signaling molecules in mammalian cells, which comprise a highly dynamic, diverse, and complex bioactive molecules [17, 18, 55]. Sphingosine-1-phosphate (S1P), as the active pro-survival product of sphingolipids, is synthesized by sphingosine kinase 1 (SphK1) and 2 (SphK2) through phosphorylation of sphingosine. S1P functions in both intra- and extracellular mechanisms that promote cell proliferation, differentiation, survival, and migration. In addition, specific transporters translocate S1P outside the cell, where it binds to sphingosine-1-phosphate receptor type 1-5 (S1PR1-5) [15, 26, 27]. The SphK/S1P/S1PR axis plays an important role in a variety of physiologic hepatic processes, and dysregulation of S1P metabolism and signaling occurs in a number of pathologic conditions, including MASLD and HCC. However, the impact of S1P on hepatic function is controversial depending on the liver cell type and S1PR expression profile [26, 40]. Therefore, the role of S1P in liver regeneration is not fully understood.

In this study, we induced the accumulation of LDs by MCD-diet and then performed 50% PHx in C57BL/6 mice. Hepatocyte proliferation was examined by monitoring the expression of specific cell cycle markers using immunohistochemistry. LD accumulation was examined using oil Red-O (ORO) staining. MCD-diet induced hepatic lipid overload accelerated liver regeneration after PHx. This finding was related to increased expression of SphK1 and neutrophil migration that served to maintain inflammatory and regenerative functions. Our findings suggest that hepatic steatosis and inflammation affect liver regeneration via the SphK1/S1P/S1PR2 axis.

II. Materials and Methods

Chemicals and biochemicals

Paraformaldehyde (PFA) was purchased from Merck (Darmstadt, Germany). Bovine serum albumin (BSA), 3-aminopropyl-triethoxysilane, tyramine hydrochloride, and Brij L23 were purchased from Sigma Chemical Co. (St Louis, MO, USA). Click-iT Cell Reaction Buffer kit, fluorescein isothiocyanate (FITC) and rhodamine-succinimidyl esters were purchased from Invitrogen (California, USA). 3,3'-Diaminobenzidine-4 HCl (DAB) was purchased from Dojindo Chemicals (Kumamoto, Japan) and 4',6-diamidino-2-phenylindole (DAPI) was purchased from Thermo Fisher (USA). 5-Ethynyl-2'-deoxyuridine (EdU) was purchased from TCI Chemicals (Tokyo, Japan). The MCD-diet was purchased from Oriental Yeast Co., Ltd. (Tokyo, Japan). All other reagents used in this study were purchased from Fujifilm Wako Pure Chemicals (Osaka, Japan).

Animals and tissue preparation

Eight-week-old, male C57BL/6 WT mice weighing 22–26 g were used in the present study. The mice were randomly divided into two groups, one of which was fed standard chow-diet (control group) and the other the MCD-diet (hepatic steatosis model group) for 2 weeks. Food and water were provided *ad libitum*, and mice were kept under specific pathogen-free conditions with a constant 12 hr dark/light cycle. The experimental protocol was approved by the Animal Ethics Review Committee of the University of Miyazaki (2018-510-7), and all experiments were performed according to the institutional guidelines of the Animal Experiment Committee.

After feeding for 2 weeks, mice were anesthetized by inhalation of isoflurane, and 50% PHx was performed by resection of the left posterior and right anterior segments

using a previously described technique [2, 4, 20, 52]. After PHx, mice were sacrificed at 0, 3, 6, 12, 24, 36, 48, 72, 120, and 168 hr, for tissue sampling as described below. All mice were injected with EdU 2 hr before euthanasia. Collected liver tissue was cut into several small pieces, some of which were snap frozen and kept at −80°C until quantitative-polymerase chain reaction (qPCR) or lipid extraction. Other pieces of liver tissue were embedded in OCT compound (Sakura Finetek, Tokyo, Japan) to prepare fresh frozen liver sections. The final remaining pieces of liver tissue were fixed overnight at room temperature in 4% PFA in phosphate-buffered saline (PBS) and subsequently embedded in paraffin using standard methods. Blood was collected via cardiac puncture and then centrifuged (2 min, 12,000 rpm, 4°C) to prepare serum, which was then stored at −80°C. A total of 6 to 8 mice were used in each experimental.

Immunohistochemistry

Paraffin-embedded tissues were cut into 5-μm-thick sections and placed onto silane-coated slide glasses. The sections were deparaffinized with toluene and rehydrated using a graded ethanol series, then autoclaved at 120°C for 15 min in 10 mM citrate buffer (pH 6.0) [12, 16, 22, 30]. After inhibition of endogenous peroxidase activity by immersion in 0.3% H_2O_2 in methanol for 15 min, the sections were pre-incubated with 500 μg/mL normal goat IgG and 1% BSA in PBS for 1 hr to block non-specific binding of antibodies. The sections were then reacted with the following primary antibodies for 16–17 hr: anti-proliferating cell nuclear antigen (PCNA) (Dako, M0879), anti-FAT/CD36 (Novus Biologicals, NB400-144), anti-S1PR2 (Novus Biologicals, NBP2-26691), anti-HNF-4α (Abcam, ab181614), anti-F4/80 (Abcam, ab6640), and anti-Ly6G (Biolegend, #127605). After washing with 0.075% Brij L23 in PBS, the sections were reacted with horseradish peroxidase (HRP)-goat anti-rabbit IgG, HRP-goat anti-mouse IgG or HRP-goat anti-rat IgG for 1 hr. After washing in 0.075% Brij/PBS, the HRP activity was visualized using DAB and H_2O_2 (brown) [47, 51]. For immunofluorescence, sections were treated with FITC-conjugated tyramide and then microwaved at 95°C for 15 min in 10 mM citrate buffer (pH 6.0). Then, next primary antibody was reacted for overnight and repeated its detection with rhodamine-conjugated tyramide and then counterstained with DAPI [6, 13, 45]. As a negative control in each experiment, normal mouse, rabbit, or rat IgG was used at the same concentration instead of the primary antibody. EdU was detected using a click-iT Cell Reaction Buffer kit, according to the manufacturer's instructions. EdU-positive hepatocytes were defined as cells with large round nuclei in DAPI staining. Microphotographs were taken using a light microscope (Olympus BX53) and Keyence BZ-X700 microscope with DAPI (excitation 360 nm), FITC (excitation 470 nm), and tetramethylrhodamine–isothiocyanate (excitation 545 nm) filters.

Lipid analysis

Hepatic fat accumulation was determined by ORO staining. Briefly, liver cryosections (5-μm-thick) were fixed with 4% PFA in PBS for 20 min and incubated in freshly prepared ORO working solution (Fujifilm Wako Pure Chemical Corp., Osaka, Japan) for 10 min and counterstained with hematoxylin for 15 sec. Random images of each ORO-stained frozen liver tissue section (n = 4 per group) were captured at ×200 magnification. The relative area of steatosis, expressed as percent fat accumulation, was quantified by histomorphometry using ImageJ software (NIH, Bethesda, Maryland, USA). Moreover, total hepatic lipids were extracted from fresh frozen liver tissue using a lipid extraction kit (STA-612; Cell Biolabs, San Diego, CA, USA). Triglycerides, cholesterol, and fatty acids in the liver and serum were quantitated using colorimetric assay kits according to the manufacturer's instructions (Fujifilm Wako) [44].

qPCR analysis

Total RNA was extracted from snap-frozen liver tissues using Isogen II (Nippon Gene, Tokyo, Japan). Total RNA was also extracted from primary cells (macrophages and neutrophils) using Reliaprep RNA Cell Miniprep System kits according to the manufacturer's instructions (Promega, USA), as reported previously [14]. RNA was reverse transcribed to cDNA using Moloney murine leukemia virus reverse transcriptase (Invitrogen). Transcript expression levels were determined using an ABI StepOne plus Real-Time PCR system (Applied Biosystems, Waltham, MA, USA) with Fast SYBR Green (Applied Biosystems). β-Actin was used for normalization, and relative gene expression in snap frozen liver tissues was calculated using the $2^{-\Delta\Delta ct}$ method, but GAPDH was used for primary cells. The primer pairs used for qPCR analyses are listed in Supplementary Table S1.

PAS staining

For glycogen detection, periodic acid-Schiff (PAS) staining was performed after PCNA staining in liver sections by incubation in 0.5% periodic acid for 5 min followed by staining with Schiff's reagent for 15 min, followed by Mayer's hematoxylin staining for 1 min. as described previously [14].

Flow cytometry

To prepare single-cell suspensions, liver tissue samples were digested with collagenase type III (Worthington Biochemical, NJ, USA) at 37°C for 30 min and then disrupted using a 100-μm cell strainer (BD Biosciences, CA, USA). Single-cell suspensions of liver cells were obtained by forcing through a 40-μm cell strainer (BD Biosciences). Macrophages and neutrophils were stained with fluorescence-conjugated monoclonal antibodies against mouse F4/80 (clone BM8, Biolegend, CA, USA) and Ly6G (clone 1A8, Biolegend) after Fc blocking with

mAb to CD16/CD32 (clone 2.4G2, BD Biosciences). S1PR2-expressing cells were stained with rabbit polyclonal antibody against S1PR2 (Novus Biologicals) followed by treatment with Alexa-633 conjugated goat anti-Rabbit IgG. Intracellular staining was performed using a fixation and permeabilization kit (eBiosciences, CA, USA). Cells were sorted with high purity (each >99%) using a FACSAria II cell sorter (BD Biosciences), and collected cells were used for further analysis.

Quantitative analysis

The number of proliferating and S1PR2-positive cells was counted in 10 random high-magnification fields per mouse using ImageJ software (NIH), as reported previously [52]. Briefly, proliferating cells are hepatocytes, and were defined as cells with large round nuclei among PCNA-positive and EdU-positive cells.

Statistical analysis

All data are expressed as the mean ± standard error of the mean (SEM). Statistical significance was assessed using Student's *t*-test. $p < 0.05$ was considered indicative of statistical significance. All analyses were performed using the Statistical Package for Social Sciences (version 20; IBM Corp., Armonk, NY, USA).

III. Results

Morphological changes in the liver of MCD-diet fed mice

The hepatic steatosis and liver regeneration model is illustrated in Figure 1A. In chow-diet fed mice, body weight increased slightly over 2 weeks. However, body weight decreased significantly in MCD-diet fed mice (Fig. 1B). After 50% PHx, the liver/body weight ratio was evaluated and results demonstrated that significant decrease in MCD-diet fed mice comparing to control mice at all timepoints. Both chow- and MCD-diet fed mice exhibited a restoration of liver weight at 168 hr after PHx (Fig. 1C).

Acceleration of hepatocyte proliferation in the liver of MCD-diet fed mice

The hepatocyte proliferation, differentiation, and apoptosis are crucial for liver regeneration. We examined cell proliferation by immunohistochemistry using specific cell cycle markers. Peak expression of PCNA, a marker of the G1/S phase, was observed at 48 hr after PHx in chow-diet fed mice livers. Interestingly, in MCD-diet fed mice, hepatocyte proliferation was accelerated, and PCNA expression was strong and peaked at 36 hr after PHx (Fig. 2A). The results of PCNA-positive cells revealed that hepatocyte proliferation initiated at 36 hr after PHx in the liver of chow-diet fed mice, but at 12 hr in the liver of MCD-diet fed mice. Moreover, the number of PCNA-positive cells was significantly higher at 12–72 hr in MCD-diet fed mice compared with control mice (Fig. 2B). To confirm these findings, EdU staining was performed, and the results were reproducible (Fig. 2C, D).

Increased hepatic lipid accumulation in the liver of MCD-diet fed mice

The impact of the MCD-diet on hepatic lipid accumulation during liver regeneration was examined using ORO

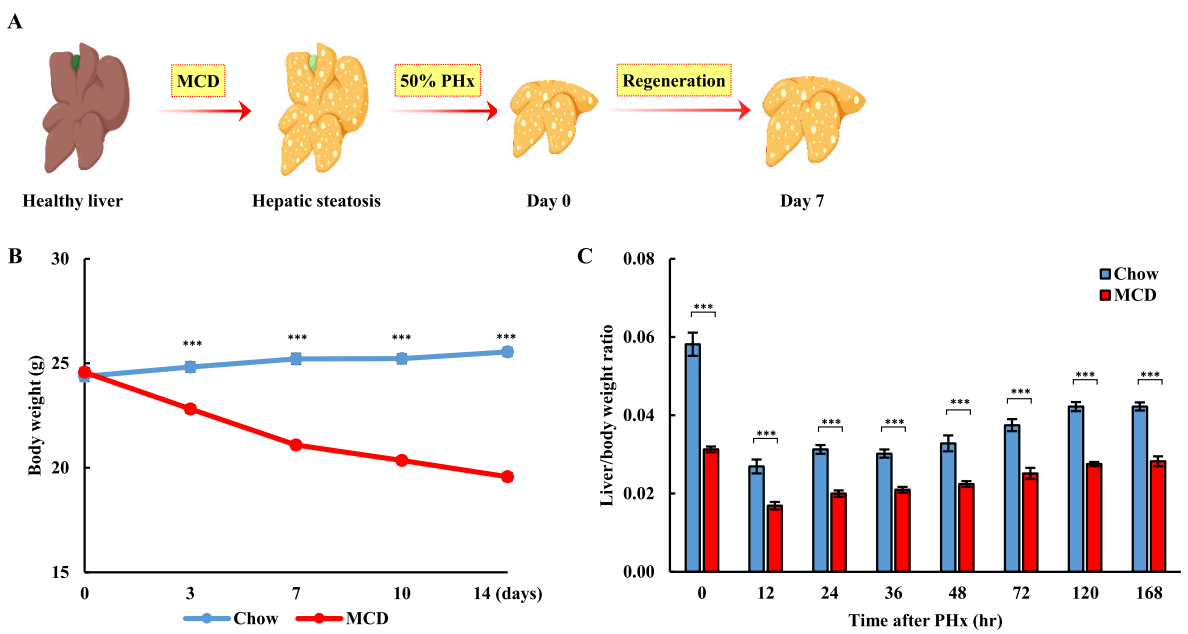

Fig. 1. Morphological changes in the liver. (**A**) Schematic illustration of the hepatic steatosis model and liver regeneration. (**B**) Body weight of chow- and MCD-diet fed mice. (**C**) Liver/body weight ratio of chow- and MCD-diet fed mice at different timepoints after PHx. Data represent the mean ± SEM for 6–8 mice. Asterisks indicate statistically significant differences (*$p < 0.05$, **$p < 0.01$ and ***$p < 0.001$).

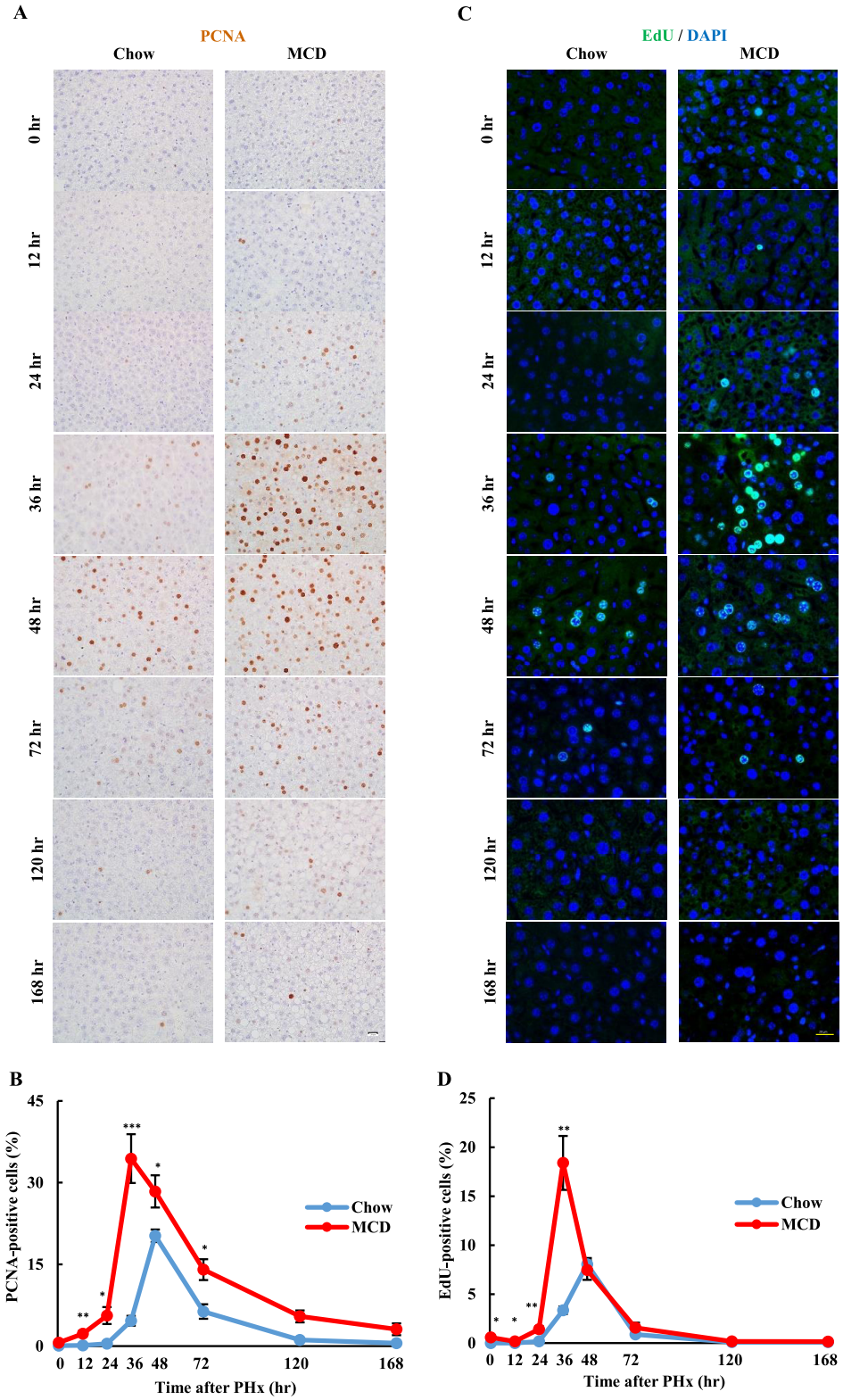

Fig. 2. Hepatocyte proliferation in mouse liver during liver regeneration. (**A**) Immunohistochemistry analysis of PCNA (brown) in the liver of chow- and MCD-diet fed mice after PHx. Bar = 20 μm; 40× objective lenses were used. Number of PCNA-positive cells (**B**) and EdU-positive cells (**D**) in the liver of chow- and MCD-diet fed mice. (**C**) Immunofluorescence analysis of EdU (green) and DAPI (blue) in mouse liver after PHx. Bar = 20 μm. Data represent the mean ± SEM for 6–8 mice per group. Asterisks indicate statistically significant differences (*$p < 0.05$, **$p < 0.01$ and ***$p < 0.001$).

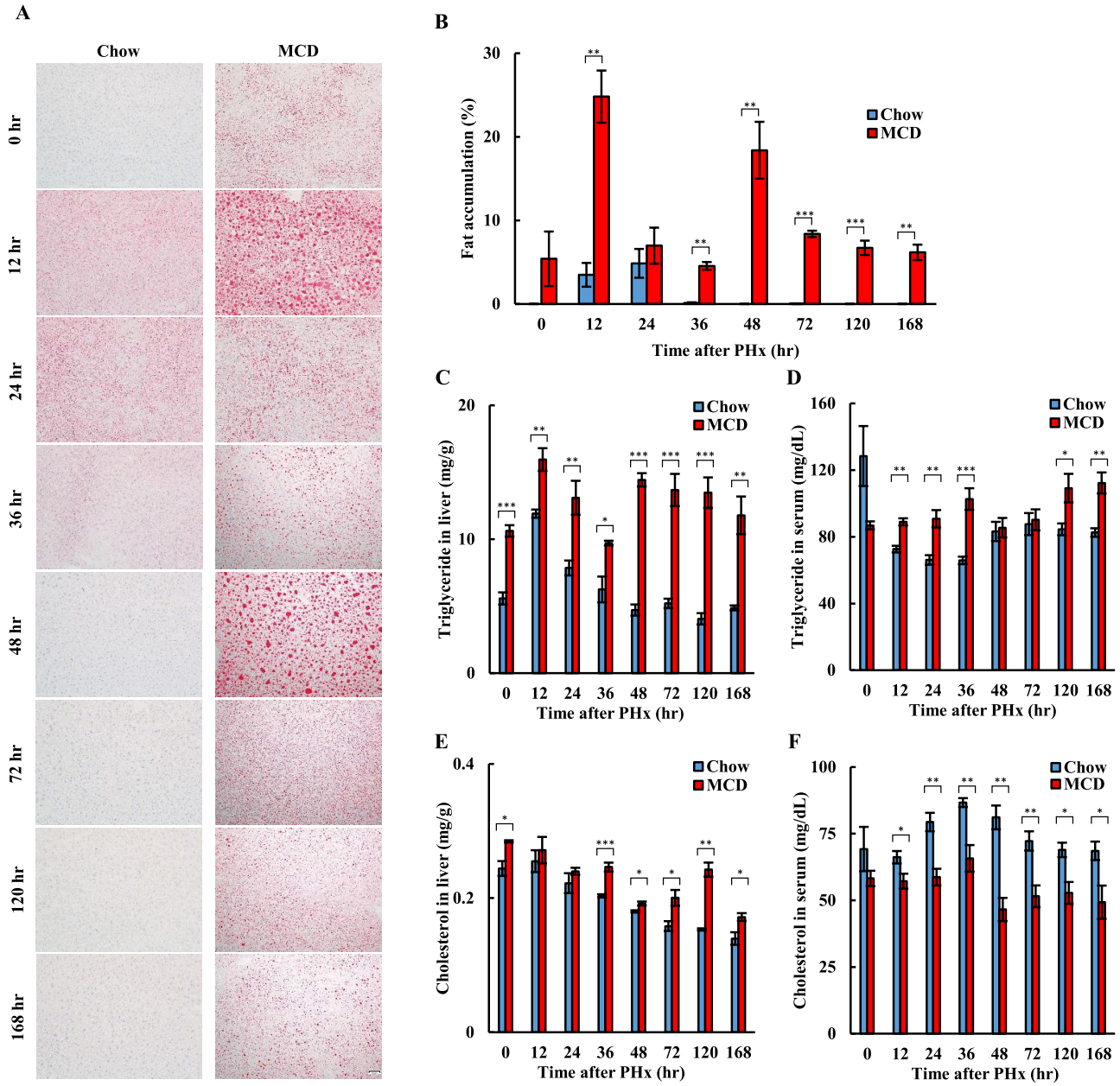

Fig. 3. Lipid accumulation in mouse liver at different timepoints after PHx. (**A**) Lipid accumulation in hepatocytes following PHx in chow- and MCD-diet fed mice was examined by ORO staining. Magnification 200×. Bar = 50 μm. (**B**) Quantitative analysis of fat deposition as a percentage of red-stained area compared with the total section area in ORO-stained liver tissue sections. Levels of (**C**, **D**) triglycerides and (**E**, **F**) cholesterol in liver and serum, respectively, during liver regeneration were assessed using enzymatic assays. Data represent the mean ± SEM for 6–8 mice per group. Asterisks indicate statistically significant differences (*p < 0.05, **p < 0.01 and ***p < 0.001).

staining. During liver regeneration, transient lipid accumulation was observed between 12–36 hr in chow-diet fed mice, but it was continuously detected in MCD-diet fed mice (Fig. 3A). Quantitative analysis revealed that the liver of MCD-diet fed mice exhibited significantly greater lipid accumulation at all timepoints than chow-diet fed mice. In contrast, changes in LDs were observed in two cycles in MCD diet-fed mice, with the first cycle occurring between 12–36 hr, and after S-phase, the second cycle was initiated at 48 hr (Fig. 3B). On the other hand, hepatic glycogen deposition or depletion is an important metabolic factor affecting hepatocyte proliferation during liver regeneration [14]. PAS and PCNA staining were performed to investigate glycogen deposition and cell proliferation, respectively. Notably, glycogen-depleted cells expressed PCNA. Additionally, the cycle of hepatic glycogen deposition and depletion alternated with the changes in lipid accumulation in the early stage of liver regeneration (Supplementary Fig. S1).

Next, we examined the quantitative analysis of lipid

components in livers and serum. Triglycerides levels were significantly elevated in both the liver and serum at all timepoints in MCD-diet fed mice compared to control mice, but which was decreased only in the serum before PHx (Fig. 3C, D). Cholesterol levels in the liver of MCD-diet fed mice were significantly higher than in chow-diet fed mice livers, particularly at 0, 36, 48, 72, 120 and 168 hr (Fig. 3E). However, serum cholesterol levels were significantly lower in MCD-diet fed mice during liver regeneration (Fig. 3F).

Analysis of fatty acids after PHx

FAT/CD36 is a major fatty acid transporter protein expressed in hepatocytes. Therefore, we analyzed the expression of FAT/CD36 using immunohistochemistry and qPCR. In the liver of MCD-diet fed mice, the intensity of FAT/CD36 staining was slightly higher compared with the liver of chow-diet fed mice (Fig. 4A). qPCR analysis revealed significantly higher expression of *FAT/CD36* mRNA in liver of MCD-diet fed mice during liver regeneration (Fig. 4B). To confirm these findings, fatty acid levels were evaluated in the liver and serum. Fatty acid levels in both the liver and serum were significantly higher in MCD-diet fed mice than in chow-diet fed mice (Fig. 4C, D).

SphK1/S1P signaling in the liver of MCD-diet fed mice after PHx

SphK1/S1P/S1PR signaling plays a critical role in cell proliferation, differentiation and survival [26]. We therefore analyzed the expression of *SphK1* and *Sphk2* mRNA in liver using qPCR. Expression of *SphK1* mRNA was upregulated in the liver of MCD-diet fed mice compared with chow-diet fed mice, particularly significant differences observed at 12, 24, 36 and 72 hr. In the normal state at 0 hr, MCD-diet fed mice expressed higher levels of *SphK1* mRNA than chow-diet fed mice. Moreover, the expression of *SphK1* mRNA was 3-fold higher in the liver of MCD-diet fed mice compared with control mice at 12 hr after PHx (Fig. 5A). Interestingly, *SphK2* mRNA expression was downregulated in the liver of both MCD- and chow-diet fed mice after PHx (Fig. 5B). Therefore, we examined expression of S1PR2, is one of the S1P receptor using immunofluorescence analysis. In the normal state, no S1PR2 expression was detected in the liver of either MCD- or chow-diet fed mice, but expression was observed beginning at 12 hr after PHx. In addition, S1PR2 staining intensity was stronger in the liver of MCD-diet fed mice at 12 hr after PHx and gradually declined between 12 and 36 hr before peaking at 72 hr (Fig. 5E). Quantitative analysis demonstrated that the number of S1PR2-positive cells was significantly higher in the liver of MCD-diet fed mice at 12, 48 and 72 hr compared with chow-diet fed mice (Fig. 5F). However, qPCR results indicated a decrease in expression of the S1PR3 and ABCC1 genes in the liver of MCD-diet fed mice during early stage of hepatectomy-induced liver regeneration. (Fig. 5C, D).

We then examined the relationship between the SphK1/S1PR2 axis and liver expression of growth factors, such as HGF and FGF2. As expected, the expression of *HGF* mRNA was significantly upregulated in the liver of MCD-diet fed mice at 0, 12, 36, 48 and 72 hr compared with control mice. Surprisingly, SphK1/S1PR2 axis and expression of *HGF* and *FGF2* mRNAs were significantly upregulated in MCD-diet fed mice at 12 hr after PHx (Fig. 6A, C). In the liver of MCD-diet fed mice, *c-Met* mRNA expression declined during the early stage of cell proliferation (Fig. 6B).

Expression of S1PR2 in mouse liver after PHx

The presence of S1PR2 was examined using double immunofluorescence together with parenchymal and non-parenchymal cell markers. In the liver of MCD-diet fed mice, S1PR2 co-localized with F4/80 (Kupffer cells) and Ly6G (neutrophils), but not with HNF-4α (hepatocytes). Interestingly, all Ly6G-positive cells were co-localized with S1PR2, whereas Kupffer cells partially expressed S1PR2. These results indicate that S1PR2 is expressed in non-parenchymal cells but not in parenchymal tissues (Fig. 7). In addition, S1PR2 did not co-localize with other non-parenchymal cells, such as desmin (quiescent hepatic stellate cells), α-SMA (activated hepatic stellate cells), Pax5 (B cells), or CD3 (T-cells) (data not shown).

S1PR2-positive cells produce growth factors during early liver regeneration

For more-detailed analyses, S1PR2-positive cells were isolated using fluorescence-activated cell sorting (FACS). PCNA-positive cells were detected as early as 12 hr after PHx in MCD-diet fed mice (Fig. 2A). Therefore, we obtained mouse liver specimens at 0, 6, and 12 hr for FACS analysis. The liver of MCD-diet fed mice contained higher numbers of neutrophils and macrophages after PHx than chow-diet fed mice (Fig. 8A). Indeed, there was no difference in the percentage of macrophages between groups at 0 hr, but the percentage of macrophages was increased in the liver of MCD-diet fed mice at 12 hr compared with chow-diet fed mice. Additionally, PHx-induced macrophage infiltration of the livers not observed in both groups (Fig. 8B). In the normal state 0 hr, the percentage of neutrophils in the liver was 4-fold higher in MCD-diet fed mice than control mice. Moreover, PHx-induced neutrophil infiltration of the liver was higher in MCD-diet fed mice (Fig. 8C).

Next, we analyzed the expression of genes encoding regenerative growth factors in macrophages and neutrophils using qPCR. The results demonstrated that expression of *HGF* and *FGF2* mRNA was significantly upregulated in macrophages isolated from the liver of MCD-diet fed mice in the normal state. Moreover, peak expression of *HGF* mRNA was observed at 6 hr with a significant difference at each timepoint (Fig. 8D), whereas *FGF2* mRNA level was significantly elevated at 12 hr compared with macrophages

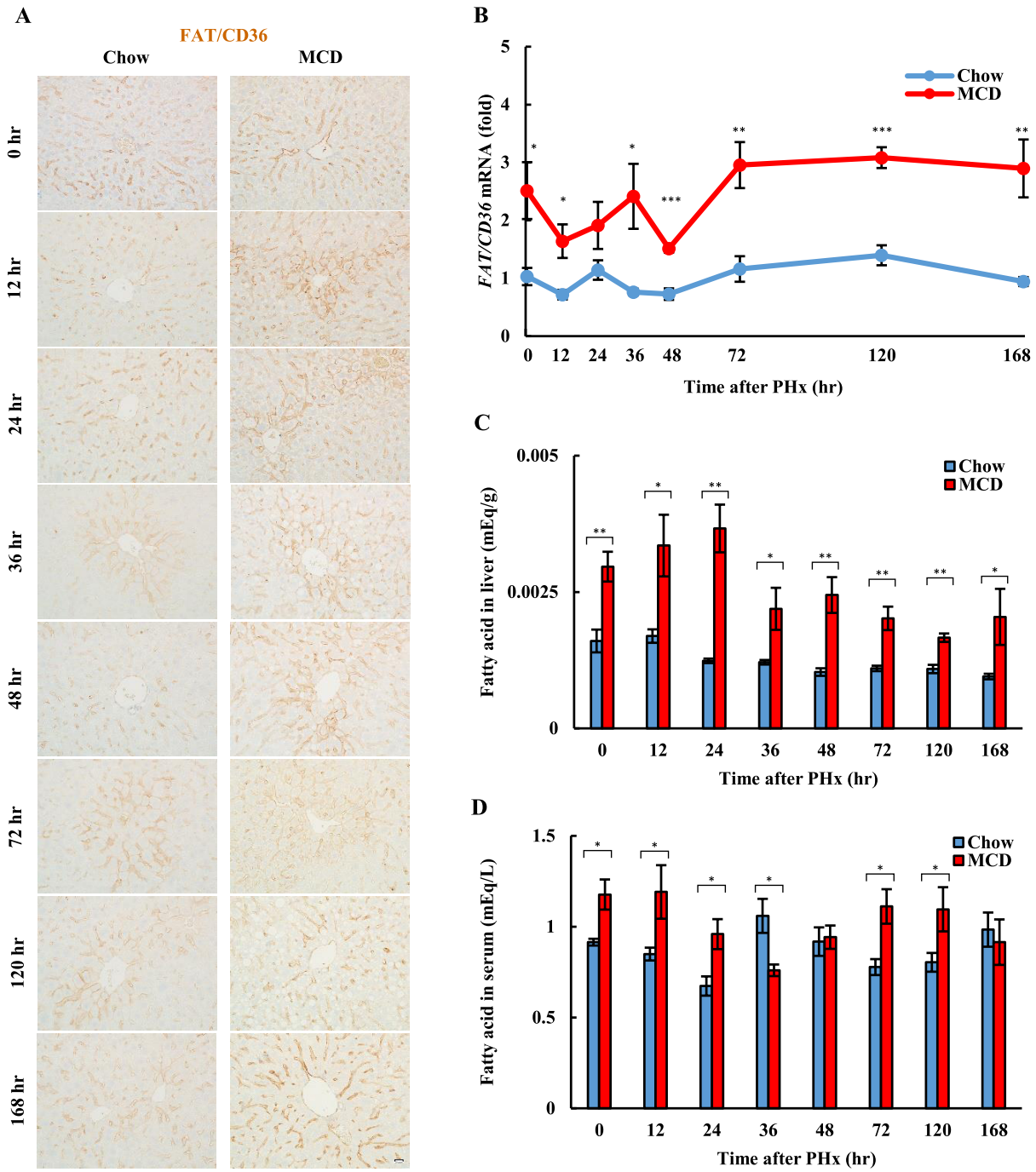

Fig. 4. Analysis of fatty acids in mouse liver following PHx. (**A**) Immunohistochemistry analysis of FAT/CD36 (brown) in the liver of chow- and MCD-diet fed mice during liver regeneration. Bar = 20 μm; 40× objective lenses were used. (**B**) qPCR analysis of *FAT/CD36* expression in mouse liver after PHx. (**C**, **D**) Levels of fatty acids in liver and serum during liver regeneration were assessed using enzymatic assays. Data represent the mean ± SEM for 6–8 mice per group. Asterisks indicate statistically significant differences (*p < 0.05, **p < 0.01 and ***p < 0.001).

isolated from the liver of chow-diet fed mice (Fig. 8F). Neutrophils initiated to secrete growth factors at 6 hr after PHx. *HGF* mRNA expression was upregulated 7-fold in neutrophils isolated from the liver of MCD-diet fed mice at 6 hr after PHx, and expression was significantly higher at all timepoints (Fig. 8E). Similarly, expression of *FGF2* mRNA was 9-fold higher and significantly different in neutrophils isolated from the liver of MCD-diet fed mice at 6 hr comparing to control mice (Fig. 8G). In addition, no changes in mRNA levels of other factors (e.g., *TNFα*, *PDGF*, and *IL-6*) were observed in macrophages and neutrophils during early liver regeneration (data not shown).

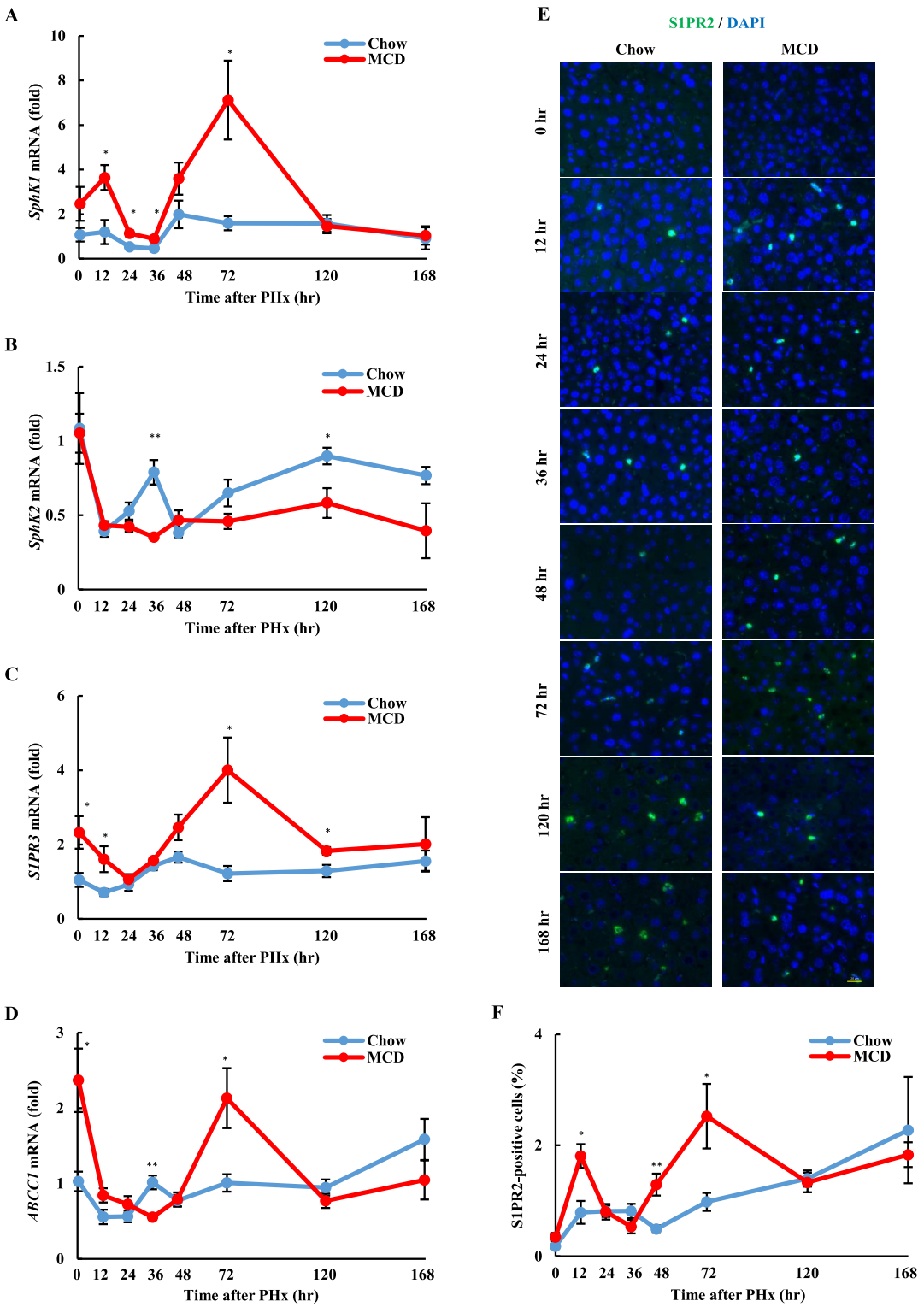

Fig. 5. SphK1/S1P signaling in mouse liver during regeneration. qPCR analysis of (**A**) *SphK1*, (**B**) *SphK2*, (**C**) *S1PR3*, and (**D**) *ABCC1* mRNA expression in the liver of chow- and MCD-diet fed mice after PHx. (**E**) Immunofluorescence analysis of S1PR2 (green) and DAPI (blue) in mouse liver after PHx. Bar = 20 μm; 40× objective lenses were used. (**F**) Quantitative analysis of S1PR2-positive cells in the liver of chow- and MCD-diet fed mice after PHx. Data represent the mean ± SEM for 6–8 mice per group. Asterisks indicate statistically significant differences (*$p < 0.05$, **$p < 0.01$ and ***$p < 0.001$).

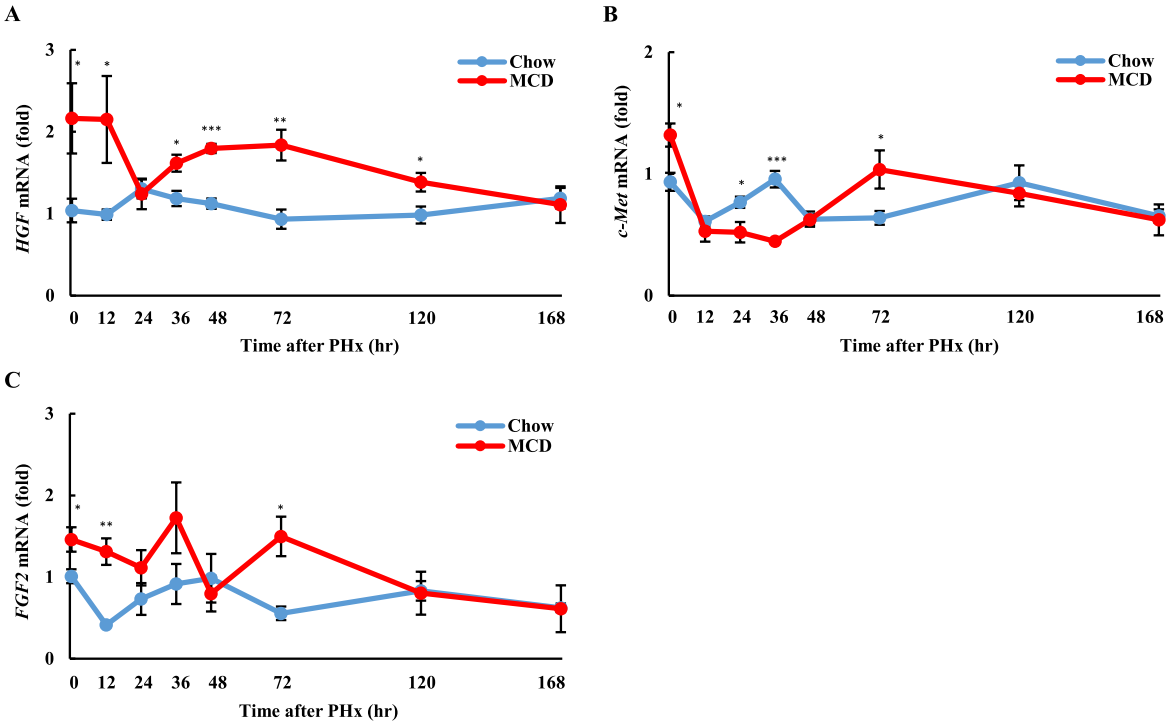

Fig. 6. Expression of regenerative growth factors in mouse liver after PHx. (**A**) *HGF*, (**B**) *c-Met*, and (**C**) *FGF2* mRNA expression levels were determined using qPCR in the liver of chow- and MCD-diet fed mice after PHx. Data represent the mean ± SEM for 6–8 mice per group. Asterisks indicate statistically significant differences (*p < 0.05, **p < 0.01 and ***p < 0.001).

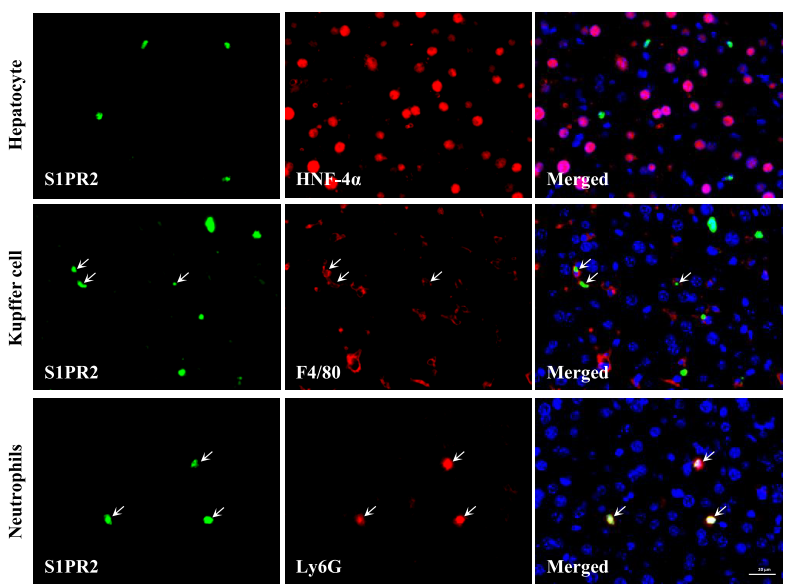

Fig. 7. Expression of S1PR2 in mouse liver. Double immunofluorescence analysis of S1PR2 (green) and HNF-4α (red staining in upper panel), F4/80 (red staining in middle panel), Ly6G (red staining in lower panel), and DAPI (blue) in the liver of MCD-diet fed mice at 12hr after PHx. Arrows indicate double-positive cells. Bar = 20 μm.

Taken together, all these results demonstrated that hepatic lipid overload promotes expression of HGF and FGF2 secreted by macrophages and neutrophils via the SphK1/S1PR2 axis to accelerate hepatocyte proliferation during liver regeneration.

IV. Discussion

The major finding of this study is that hepatic lipid accumulation accelerates liver regeneration after PHx. Our study provides the following findings: (1) accumulation of

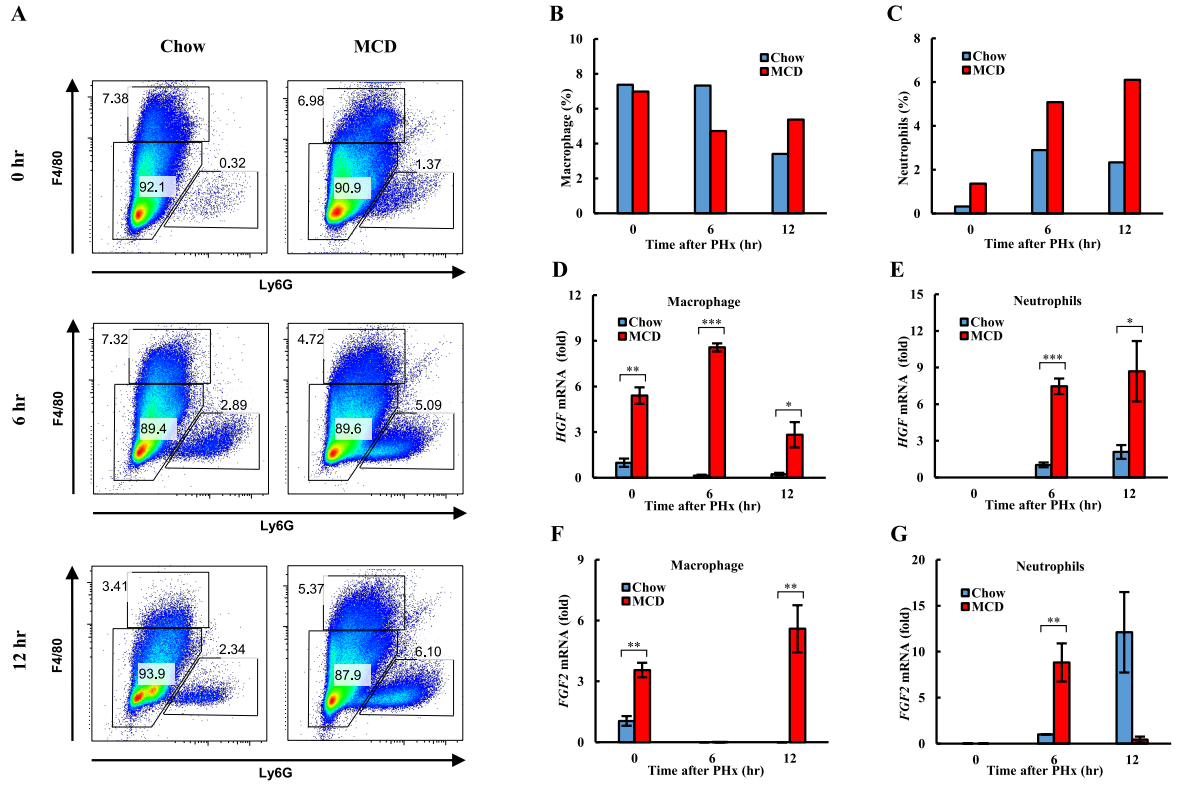

Fig. 8. *HGF* and *FGF2* mRNA expression in S1PR2-positive cells after PHx. (**A**) Macrophages (F4/80) and neutrophils (Ly6G) were isolated from the liver of chow- and MCD-diet fed mice at 0, 6, and 12 hr after PHx. The percentage of macrophages (**B**) and neutrophils (**C**) in the liver of chow- and MCD-diet fed mice. *HGF* and *FGF2* mRNA expression levels in (**D**, **F**) macrophages and (**E**, **G**) neutrophils isolated from the liver of chow- and MCD-diet fed mice at 0, 6 and 12 hr after PHx. Data represent the mean ± SEM for 3 mice per group. Asterisks indicate statistically significant differences (*p < 0.05, **p < 0.01 and ***p < 0.001).

LDs is correlated with the proliferative activity of hepatocytes; (2) the SphK1/S1P/S1PR2 signaling pathway is activated in neutrophils and macrophages during early liver regeneration; and (3) HGF and FGF2 are secreted by neutrophils and macrophages.

Both body weight and the liver/body weight ratio were significantly decreased in MCD-diet fed mice in the present study. Our results confirmed that hepatocyte lipid accumulation and early inflammation exhibit in MCD-diet fed animals within 2 weeks, and pericellular, perisinusoidal fibrosis in 8 – 10 weeks, whereas 40% weight loss in 8–10 weeks feeding [8, 29, 36, 49]. Additionally, the MCD-diet model closely simulates the histopathologic features of human MASH within a comparably shorter time than other dietary models of MASH, which has the advantage of effectively and reproducibly introducing hepatic steatosis and inflammation in animals [19, 29].

After PHx, the remnant liver exhibits different survival action depending on the extent of surgery; both cell proliferation and hypertrophy appear after 70% PHx, whereas only hypertrophy observed after 30% PHx [31, 50]. Activation of G0/G1 transition recruits 95% account of hepatocytes to initiate the cell cycle and become ready for mitosis during the priming phase [32, 35]. Our results of the proliferative activity of hepatocytes revealed significantly accelerated liver regeneration in MCD-diet fed mice, suggesting that accelerated hepatocyte proliferation is correlated with hepatic steatosis. Zou *et al.* demonstrated that four waves of hepatocyte proliferation are coupled to three waves of hepatic fat accumulation during liver regeneration after PHx [56]. In our previous and current studies, we found that expression of FAT/CD36, a key fatty acid transporter, is closely related to active hepatocyte proliferation [14, 44]. Indeed, in the present study, the lipid contents of the liver and serum were significantly higher in MCD-diet fed mice at all timepoints after PHx, whereas glycogen-depleted areas were observed in proliferating hepatocytes during liver regeneration. Inconsistent results were reported previously, such as many studies linked with mild hepatic steatosis being improved or not impaired for liver regeneration in experimental animals [11, 41, 46]. Despite these findings, severe steatosis was shown to induce hepatocellular injury and impaired liver regeneration in a MASLD/MASH model [23, 49]. The differences between these results might be due to differences in factors such as the severity of hepatic steatosis, the volume of remnant liver, and the type of food used to induce steatosis.

Fatty acids, particularly palmitate, serve as a primary

source of bioactive sphingolipids, with elevated levels in the liver and serum observed during MASLD progression [1, 55]. Numerous studies have reported that hepatic expression of SphK1 is elevated in both MASLD and advanced-grade HCC, which directly indicates increased production of S1P [28, 42]. In addition, Chen *et al.* revealed that deletion of SphK1 inhibits the proliferation of liver cancer cells, as examined based on expression levels of PCNA and cyclin D1 [10]. In our study, the SphK1/S1P/S1PR2 signaling pathway was significantly upregulated in the liver of MCD-diet fed mice after PHx. Collectively, these findings suggest that the SphK1/S1P/S1PR2 signaling pathway promotes hepatocyte proliferation during liver regeneration in steatotic liver. In contrast, upregulation of the SphK1/S1PR2 axis does not affect liver regeneration but instead triggers matrix remodeling during hepatic wound healing induced by acute liver injury [43]. Despite these findings, Ikeda *et al.* reported enhanced liver regeneration in S1PR2-knockout mice after liver injury, with an increase in the number of PCNA-positive hepatocytes, whereas decrease in PCNA-positive non-parenchymal cells [21]. These differing phenomena may be the result of several factors, including the liver regeneration models used, the time period examined in the models, and the use of specific gene-knockout mice.

Furthermore, according to results the S1PR2 was expressed in non-parenchymal cells, such as neutrophils and Kupffer cells in regenerating liver of MCD-diet fed mice. Indeed, S1PR2-mediated neutrophil activation plays an important role in liver injury during the early stage of MASLD [53]. However, activation of non-parenchymal cells to initiate the liver regeneration after PHx, and the resulting cellular interactions are regulated by the release of various growth factors and cytokines [24, 35]. Neutrophils release growth factors such as HGF and FGF2 [5]. HGF is a key growth factor secreted by mesenchymal cells, and it is expressed in two stages, a depletion phase from 0–3 hr and a production phase from 3–48 hr after PHx [54]. In addition, FGF2 stimulates a moderate amount of DNA synthesis in rat hepatocyte culture [33]. Similar to the above facts, our results revealed that significant increases in *HGF* and *FGF2* expression in the liver of MCD-diet fed mice during early regeneration.

Our S1PR2-positive cell isolation experiment confirmed that *HGF* and *FGF2* expression was significantly upregulated in neutrophils and macrophages isolated from the liver of MCD-diet fed mice. Nachmany *et al.* demonstrated that Ly6G-positive cells promote early liver regeneration in a murine model of major hepatectomy [34]. A similar study reported that neutrophil-released factors support hepatocytes with a pro-regenerative potential after PHx [5].

In conclusion, the present study demonstrated that hepatic steatosis accelerates liver regeneration after PHx and induces the recruitment of neutrophils and macrophages with regenerative potential to release HGF and FGF2 via the SphK1/S1PR2 signaling pathway. Our findings might contribute to the understanding of promoting regeneration in the steatotic liver.

V. Conflicts of Interest

We have no conflict of interest to declare.

VI. Acknowledgments

This study was supported in part by a Grant-in-Aid for Scientific Research from the Japan Society for the Promotion of Science (No. 21K06738 to YH., No. 19K16477 to NC.). We gratefully acknowledge the Frontier Science Research Center at the University of Miyazaki for allowing us to use their facilities.

VII. References

1. Al Fadel, F., Fayyaz, S., Japtok, L. and Kleuser, B. (2016) Involvement of Sphingosine 1-Phosphate in Palmitate-Induced Non-Alcoholic Fatty Liver Disease. *Cell Physiol. Biochem.* 40; 1637–1645.
2. Anderson, R. and Higgins, G. (1931) Experimental pathology of the liver. I. Restoration of the liver of the white rat following partial surgical removal. *Arch. Pathot.* 12; 186–202.
3. Arrese, M., Cabrera, D., Kalergis, A. M. and Feldstein, A. E. (2016) Innate Immunity and Inflammation in NAFLD/NASH. *Dig. Dis. Sci.* 61; 1294–1303.
4. Batmunkh, B., Choijookhuu, N., Srisowanna, N., Byambatsogt, U., Synn Oo, P., Noor Ali, M., *et al.* (2017) Estrogen Accelerates Cell Proliferation through Estrogen Receptor alpha during Rat Liver Regeneration after Partial Hepatectomy. *Acta Histochem. Cytochem.* 50; 39–48.
5. Brandel, V., Schimek, V., Gober, S., Hammond, T., Brunnthaler, L., Schrottmaier, W. C., *et al.* (2022) Hepatectomy-induced apoptotic extracellular vesicles stimulate neutrophils to secrete regenerative growth factors. *J. Hepatol.* 77; 1619–1630.
6. Buchwalow, I., Samoilova, V., Boecker, W. and Tiemann, M. (2018) Multiple immunolabeling with antibodies from the same host species in combination with tyramide signal amplification. *Acta Histochem.* 120; 405–411.
7. Caldez, M. J., Bjorklund, M. and Kaldis, P. (2020) Cell cycle regulation in NAFLD: when imbalanced metabolism limits cell division. *Hepatol. Int.* 14; 463–474.
8. Carril, E., Valdecantos, M. P., Lanzon, B., Angulo, S., Valverde, A. M., Godzien, J., *et al.* (2020) Metabolic impact of partial hepatectomy in the non-alcoholic steatohepatitis animal model of methionine-choline deficient diet. *J. Pharm. Biomed. Anal.* 178; 112958.
9. Chalasani, N., Younossi, Z., Lavine, J. E., Diehl, A. M., Brunt, E. M., Cusi, K., *et al.* (2012) The diagnosis and management of non-alcoholic fatty liver disease: practice Guideline by the American Association for the Study of Liver Diseases, American College of Gastroenterology, and the American Gastroenterological Association. *Hepatology* 55; 2005–2023.
10. Chen, J., Qi, Y., Zhao, Y., Kaczorowski, D., Couttas, T. A., Coleman, P. R., *et al.* (2018) Deletion of sphingosine kinase 1 inhibits liver tumorigenesis in diethylnitrosamine-treated mice. *Oncotarget* 9; 15635–15649.
11. Chen, Y., Chen, L., Wu, X., Zhao, Y., Wang, Y., Jiang, D., *et al.* (2023) Acute liver steatosis translationally controls the

epigenetic regulator MIER1 to promote liver regeneration in a study with male mice. *Nat Commun.* 14; 1521.
12. Choijookhuu, N., Sato, Y., Nishino, T., Endo, D., Hishikawa, Y. and Koji, T. (2012) Estrogen-dependent regulation of sodium/hydrogen exchanger-3 (NHE3) expression via estrogen receptor beta in proximal colon of pregnant mice. *Histochem. Cell Biol.* 137; 575–587.
13. Choijookhuu, N., Shibata, Y., Ishizuka, T., Xu, Y., Koji, T. and Hishikawa, Y. (2022) An Advanced Detection System for *In Situ* Hybridization Using a Fluorescence Resonance Energy Transfer-based Molecular Beacon Probe. *Acta Histochem. Cytochem.* 55; 119–128.
14. Choijookhuu, N., Yano, K., Lkham-Erdene, B., Shirouzu, S., Kubota, T., Fidya, *et al.* (2024) HMGB2 Promotes De Novo Lipogenesis to Accelerate Hepatocyte Proliferation During Liver Regeneration. *J. Histochem. Cytochem.* 72; 245–264.
15. Cui, M., Gobel, V. and Zhang, H. (2022) Uncovering the 'sphinx' of sphingosine 1-phosphate signalling: from cellular events to organ morphogenesis. *Biol. Rev. Camb. Philos. Soc.* 97; 251–272.
16. Fidya, Choijookhuu, N., Ikenoue, M., Yano, K., Yamaguma, Y., Shirouzu, S., *et al.* (2024) Protective role of estrogen through G-protein coupled receptor 30 in a colitis mouse model. *Histochem. Cell Biol.* 161; 81–93.
17. Green, C. D., Maceyka, M., Cowart, L. A. and Spiegel, S. (2021) Sphingolipids in metabolic disease: The good, the bad, and the unknown. *Cell Metab.* 33; 1293–1306.
18. Hannun, Y. A. and Obeid, L. M. (2018) Sphingolipids and their metabolism in physiology and disease. *Nat. Rev. Mol. Cell Biol.* 19; 175–191.
19. Harada, S., Taketomi, Y., Aiba, T., Kawaguchi, M., Hirabayashi, T., Uranbileg, B., *et al.* (2023) The Lysophospholipase PNPLA7 Controls Hepatic Choline and Methionine Metabolism. *Biomolecules* 13; 471.
20. Hori, T., Ohashi, N., Chen, F., Baine, A. M., Gardner, L. B., Hata, T., *et al.* (2012) Simple and reproducible hepatectomy in the mouse using the clip technique. *World J. Gastroenterol.* 18; 2767–2774.
21. Ikeda, H., Watanabe, N., Ishii, I., Shimosawa, T., Kume, Y., Tomiya, T., *et al.* (2009) Sphingosine 1-phosphate regulates regeneration and fibrosis after liver injury via sphingosine 1-phosphate receptor 2. *J. Lipid. Res.* 50; 556–564.
22. Ikenoue, M., Choijookhuu, N., Yano, K., Fidya, Takahashi, N., Ishizuka, T., *et al.* (2024) The crucial role of SETDB1 in structural and functional transformation of epithelial cells during regeneration after intestinal ischemia reperfusion injury. *Histochem. Cell Biol.* 161; 325–336.
23. Islam, S. M. T., Palanisamy, A. P., Chedister, G. R., Schmidt, M. G., Lewin, D. N. B. and Chavin, K. D. (2023) Unsaturated or saturated dietary fat-mediated steatosis impairs hepatic regeneration following partial hepatectomy in mice. *PLoS One* 18; e0284428.
24. Kimura, M., Moteki, H. and Ogihara, M. (2023) Role of Hepatocyte Growth Regulators in Liver Regeneration. *Cells* 12; 208.
25. Kitto, L. J. and Henderson, N. C. (2021) Hepatic Stellate Cell Regulation of Liver Regeneration and Repair. *Hepatol. Commun.* 5; 358–370.
26. Kleuser, B. (2018) Divergent Role of Sphingosine 1-Phosphate in Liver Health and Disease. *Int. J. Mol. Sci.* 19; 722.
27. Ksiazek, M., Chacinska, M., Chabowski, A. and Baranowski, M. (2015) Sources, metabolism, and regulation of circulating sphingosine-1-phosphate. *J. Lipid Res.* 56; 1271–1281.
28. Kwong, E. K., Li, X., Hylemon, P. B. and Zhou, H. (2017) Sphingosine Kinases/Sphingosine 1-Phosphate Signaling in Hepatic Lipid Metabolism. *Curr. Pharmacol. Rep.* 3; 176–183.
29. Li, H., Toth, E. and Cherrington, N. J. (2018) Asking the Right Questions With Animal Models: Methionine- and Choline-Deficient Model in Predicting Adverse Drug Reactions in Human NASH. *Toxicol. Sci.* 161; 23–33.
30. Masuda, S. and Nakanishi, Y. (2023) Application of Immunohistochemistry in Clinical Practices as a Standardized Assay for Breast Cancer. *Acta Histochem. Cytochem.* 56; 1–8.
31. Meier, M., Andersen, K. J., Knudsen, A. R., Nyengaard, J. R., Hamilton-Dutoit, S. and Mortensen, F. V. (2016) Liver regeneration is dependent on the extent of hepatectomy. *J. Surg. Res.* 205; 76–84.
32. Michalopoulos, G. K. (2017) Hepatostat: Liver regeneration and normal liver tissue maintenance. *Hepatology* 65; 1384–1392.
33. Michalopoulos, G. K. and Bhushan, B. (2021) Liver regeneration: biological and pathological mechanisms and implications. *Nat. Rev. Gastroenterol. Hepatol.* 18; 40–55.
34. Nachmany, I., Bogoch, Y., Sivan, A., Amar, O., Bondar, E., Zohar, N., *et al.* (2019) CD11b(+)Ly6G(+) myeloid-derived suppressor cells promote liver regeneration in a murine model of major hepatectomy. *FASEB J.* 33; 5967–5978.
35. Ozaki, M. (2020) Cellular and molecular mechanisms of liver regeneration: Proliferation, growth, death and protection of hepatocytes. *Semin. Cell Dev. Biol.* 100; 62–73.
36. Parlati, L., Regnier, M., Guillou, H. and Postic, C. (2021) New targets for NAFLD. *JHEP Rep.* 3; 100346.
37. Qu, X., Wen, Y., Jiao, J., Zhao, J., Sun, X., Wang, F., *et al.* (2022) PARK7 deficiency inhibits fatty acid beta-oxidation via PTEN to delay liver regeneration after hepatectomy. *Clin. Transl. Med.* 12; e1061.
38. Rinella, M. E., Lazarus, J. V., Ratziu, V., Francque, S. M., Sanyal, A. J., Kanwal, F., *et al.* (2023) A multisociety Delphi consensus statement on new fatty liver disease nomenclature. *J. Hepatol.* 79; 1542–1556.
39. Rinella, M. E. and Sookoian, S. (2024) From NAFLD to MASLD: updated naming and diagnosis criteria for fatty liver disease. *J. Lipid Res.* 65; 100485.
40. Rohrbach, T., Maceyka, M. and Spiegel, S. (2017) Sphingosine kinase and sphingosine-1-phosphate in liver pathobiology. *Crit. Rev. Biochem. Mol. Biol.* 52; 543–553.
41. Rudnick, D. A. and Davidson, N. O. (2012) Functional Relationships between Lipid Metabolism and Liver Regeneration. *Int. J. Hepatol.* 2012; 549241.
42. Satyananda, V., Oshi, M., Tokumaru, Y., Maiti, A., Hait, N., Matsuyama, R., *et al.* (2021) Sphingosine 1-phosphate (S1P) produced by sphingosine kinase 1 (SphK1) and exported via ABCC1 is related to hepatocellular carcinoma (HCC) progression. *Am. J. Cancer Res.* 11; 4394–4407.
43. Serriere-Lanneau, V., Teixeira-Clerc, F., Li, L., Schippers, M., de Wries, W., Julien, B., *et al.* (2007) The sphingosine 1-phosphate receptor S1P2 triggers hepatic wound healing. *FASEB J.* 21; 2005–2013.
44. Srisowanna, N., Choijookhuu, N., Yano, K., Batmunkh, B., Ikenoue, M., Nhat Huynh Mai, N., *et al.* (2019) The Effect of Estrogen on Hepatic Fat Accumulation during Early Phase of Liver Regeneration after Partial Hepatectomy in Rats. *Acta Histochem. Cytochem.* 52; 67–75.
45. Sugita, N., Choijookhuu, N., Yano, K., Lee, D., Ikenoue, M., Fidya, *et al.* (2021) Depletion of high-mobility group box 2 causes seminiferous tubule atrophy via aberrant expression of androgen and estrogen receptors in mouse testis†. *Biol. Reprod.* 105; 1510–1520.
46. Sydor, S., Gu, Y., Schlattjan, M., Bechmann, L. P., Rauen, U., Best, J., *et al.* (2013) Steatosis does not impair liver regeneration after partial hepatectomy. *Lab. Invest.* 93; 20–30.

47. Taguchi, R., Yamaguchi-Tanaka, M., Takagi, K., Sato, A., Miki, Y., Miyashita, M., *et al.* (2024) Clinicopathological Significance and Prognostic Role of High Mobility Group Box 1 (HMGB1), Toll-Like Receptor (TLR) 2 and TLR4 in Breast Cancer. *Acta Histochem. Cytochem.* 57; 75–83.
48. Tokushige, K. (2024) New concept in fatty liver diseases. *Hepatol. Res.* 54; 125–130.
49. Vetelainen, R., van Vliet, A. K. and van Gulik, T. M. (2007) Severe steatosis increases hepatocellular injury and impairs liver regeneration in a rat model of partial hepatectomy. *Ann. Surg.* 245; 44–50.
50. Yagi, S., Hirata, M., Miyachi, Y. and Uemoto, S. (2020) Liver Regeneration after Hepatectomy and Partial Liver Transplantation. *Int. J. Mol. Sci.* 21; 8414.
51. Yamaguma, Y., Sugita, N., Choijookhuu, N., Yano, K., Lee, D., Ikenoue, M., *et al.* (2022) Crucial role of high-mobility group box 2 in mouse ovarian follicular development through estrogen receptor beta. *Histochem. Cell Biol.* 157; 359–369.
52. Yano, K., Choijookhuu, N., Ikenoue, M., Fidya, Fukaya, T., Sato, K., *et al.* (2022) Spatiotemporal expression of HMGB2 regulates cell proliferation and hepatocyte size during liver regeneration. *Sci. Rep.* 12; 11962.
53. Zhao, X., Yang, L., Chang, N., Hou, L., Zhou, X., Yang, L., *et al.* (2020) Neutrophils undergo switch of apoptosis to NETosis during murine fatty liver injury via S1P receptor 2 signaling. *Cell Death Dis.* 11; 379.
54. Zhao, Y., Ye, W., Wang, Y. D. and Chen, W. D. (2022) HGF/c-Met: A Key Promoter in Liver Regeneration. *Front. Pharmacol.* 13; 808855.
55. Zhu, C., Huai, Q., Zhang, X., Dai, H., Li, X. and Wang, H. (2023) Insights into the roles and pathomechanisms of ceramide and sphigosine-1-phosphate in nonalcoholic fatty liver disease. *Int. J. Biol. Sci.* 19; 311–330.
56. Zou, Y., Bao, Q., Kumar, S., Hu, M., Wang, G. Y. and Dai, G. (2012) Four waves of hepatocyte proliferation linked with three waves of hepatic fat accumulation during partial hepatectomy-induced liver regeneration. *PLoS One* 7; e30675.

This is an open access article distributed under the Creative Commons Attribution-NonCommercial 4.0 International License (CC-BY-NC), which permits use, distribution and reproduction of the articles in any medium provided that the original work is properly cited and is not used for commercial purposes.